Article

Pyrrolidinyl Synthetic Cathinones α-PHP and 4F-α-PVP Metabolite Profiling Using Human Hepatocyte Incubations

Jeremy Carlier [1,2,3], Xingxing Diao [1,4], Raffaele Giorgetti [2], Francesco P. Busardò [2,*] and Marilyn A. Huestis [1,5]

[1] Chemistry & Drug Metabolism Section, Intramural Research Program, National Institute on Drug Abuse, National Institutes of Health, Baltimore, MD 21224, USA; jerem.carlier@gmail.com (J.C.); xxdiao@simm.ac.cn (X.D.); marilyn.huestis@gmail.com (M.A.H.)

[2] Department of Excellence of Biomedical Sciences and Public Health, Unit of Forensic Toxicology, Section of Legal Medicine, Marche Polytechnic University, 60126 Ancona, Italy; r.giorgetti@staff.univpm.it

[3] Department of Anatomical, Histological, Unit of Forensic Toxicology, Section of Legal Medicine, Forensic, and Orthopedic Sciences, Sapienza University of Rome, 00198 Rome, Italy

[4] Shanghai Institute of Materia Medica, Chinese Academy of Sciences, Shanghai 201203, China

[5] Institute of Emerging Health Professions, Thomas Jefferson University, Philadelphia, PA 19107, USA

* Correspondence: fra.busardo@libero.it

Abstract: For more than ten years, new synthetic cathinones (SCs) mimicking the effects of controlled cocaine-like stimulants have flooded the illegal drug market, causing numerous intoxications and fatalities. There are often no data on the pharmacokinetics of these substances when they first emerge onto the market. However, the detection of SC metabolites is often critical in order to prove consumption in clinical and forensic settings. In this research, the metabolite profile of two pyrrolidinyl SCs, α-pyrrolidinohexaphenone (α-PHP) and 4″-fluoro-α-pyrrolidinovalerophenone (4F-α-PVP), were characterized to identify optimal intake markers. Experiments were conducted using pooled human hepatocyte incubations followed by liquid chromatography–high-resolution tandem mass spectrometry and data-mining software. We suggest α-PHP dihydroxy-pyrrolidinyl, α-PHP hexanol, α-PHP 2′-keto-pyrrolidinyl-hexanol, and α-PHP 2′-keto-pyrrolidinyl as markers of α-PHP use, and 4F-α-PVP dihydroxy-pyrrolidinyl, 4F-α-PVP hexanol, 4F-α-PVP 2′-keto-pyrrolidinyl-hexanol, and 4F-α-PVP 2′-keto-pyrrolidinyl as markers of 4F-α-PVP use. These results represent the first data available on 4F-α-PVP metabolism. The metabolic fate of α-PHP was previously studied using human liver microsomes and urine samples from α-PHP users. We identified an additional major metabolite (α-PHP dihydroxy-pyrrolidinyl) that might be crucial for documenting exposure to α-PHP. Further experiments with suitable analytical standards, which are yet to be synthesized, and authentic specimens should be conducted to confirm these results.

Keywords: α-PHP; PV7; 4F-α-PVP; novel psychoactive substance; synthetic cathinone; bath salt; hepatocyte metabolism; liquid chromatography–high resolution tandem mass spectrometry

1. Introduction

Synthetic cathinones (SCs), or bath salts, are novel psychoactive substances (NPSs) designed to induce cocaine-like stimulant effects while evading legislation and analytical detection. SCs inhibit the transport of monoamines in the central nervous system, with specific affinities for dopamine, norepinephrine, and serotonin transporters (DAT, NET, and SERT, respectively), inducing euphoria and increased energy, but also tachycardia, elevated blood pressure, hyperthermia, agitation, delirium, psychosis, and death. SC use accounts for many intoxications and deaths, mainly through cardiac arrest or multi-organ failure [1,2]. SC effects are closely related to their specific selectivity for DAT, NET, and SERT. Particularly, DAT/SERT inhibition is associated with distinct psychoactive effects and abuse liability. For example, methedrone and 4-ethylmethcathinone have DAT/SERT inhibition ratios similar to that of 3″,4″-methylenedioxymethamphetamine

(MDMA), whereas methylenedioxypyrovalerone (MDPV) and pyrovalerone have a much higher ratio, resulting in higher reinforcing effects and abuse potential [3].

α-PHP (or PV7 or α-pyrrolidinohexaphenone, 1-phenyl-2-(1′-pyrrolidinyl)-1-hexanone) and 4F-α-PVP (or 4″-fluoro-α-pyrrolidinovalerophenone, 1-(4″-fluorophenyl)-2-(1′-pyrrolidinyl)-1-pentanone) are pyrrolidinyl SCs, characterized by the presence of a butyl chain and a phenyl for α-PHP, and a propyl chain and a *para*-fluoro-phenyl ring for 4F-α-PVP (Figure 1). Both SCs were first identified in 2014 in material seized in the Japanese illegal drug market or for sale over the Internet [4,5]. α-PHP was recently involved in several combined drug intoxication fatalities [6–10]. All the cases involved the co-ingestion of other SCs, mainly α-pyrrolidinovalerophenone (α-PVP) and 3″,4″-methylenedioxy-α-pyrrolidinohexiophenone (MDPHP), or often opiates and/or benzodiazepines. A total of 13 α-PHP-related deaths were reported to the early warning system of the European Monitoring Centre for Drugs and Drug Addiction (EMCDDA) between 2017 and 2020 [2], with additional cases reported to the United Nations Office on Drugs and Crime (UNODC) early warning advisory system [11]. No intoxication cases or deaths involving 4F-α-PVP have been reported to date. Halogenated SCs inhibit SERT with a higher potency than that of their non-halogenated analogues, inducing potentially fatal serotonin syndrome effects—tachycardia; nausea; hyperthermia; rhabdomyolysis; psychomotor tremors; and liver, kidney, and lung failure [12–15]. Therefore, 4F-α-PVP is expected to demonstrate higher toxicity than α-PVP, which has been involved in many intoxications and fatalities [1,2]. Halogenated SC use recently became popular, likely due to its higher potency [2], and 4F-α-PVP use is also expected to increase. In December 2019, the World Health Organization (WHO) recommended the control of α-PHP under Schedule II of the UNODC convention on psychotropic substances of 1971 [16]. It is currently controlled under Class B in the United Kingdom; Schedule I in the United States; is illegal in China, Sweden, Poland, and Italy; and is classified as a narcotic in Japan [11,17]. 4F-α-PVP is illegal in China and classified as a designated chemical substance in Japan [17].
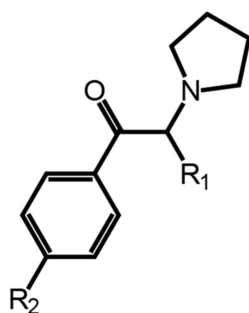
α-PPP	R_1 = CH_3	R_2 = H
α-PBP	R_1 = CH_2CH_3	R_2 = H
α-PVP	R_1 = $(CH_2)_2CH_3$	R_2 = H
4F-α-PVP	R_1 = $(CH_2)_2CH_3$	R_2 = F
4-MeO-α-PVP	R = $(CH_2)_2CH_3$	R_2 = OCH_3
α-PHP	R = $(CH_2)_3CH_3$	R_2 = H
PV8	R = $(CH_2)_4CH_3$	R_2 = H
PV9	R = $(CH_2)_5CH_3$	R_2 = H

Figure 1. Chemical structures of α-PHP, 4F-α-PVP, and structural analogues α-PPP, α-PBP, α-PVP, 4-MeO-α-PVP, PV8, and PV9.

Exposure to α-PHP can be determined through the detection of parent drugs in biological specimens [6–9]. α-PHP has been quantified in post-mortem cases with concentrations ranging from 4 to 52 ng/mL in blood [6,7], 5.6 ng/mL in urine [9], 3.5 to 83.3 ng/g in tis-

sues [9], and 4700 pg/mg in hair [8]. Although α-PHP was not the primary cause of death in these cases, active and toxic concentrations are expected to be low. 4F-α-PVP concentrations in biological specimens have not been reported to date. In clinical and forensic settings, toxicologists often focus on the detection of drug metabolites in urine, which are often detected in higher concentrations and over an extended time course. A prerequisite for the detection of metabolites is the characterization of the drug's metabolic fate. However, there are often no data on SC pharmacokinetics when they first emerge onto the illegal drug market. To date, there are no data available on 4F-α-PVP pharmacokinetics. α-PHP metabolism, however, was investigated using human liver microsomes and authentic urine samples. Several α-PHP metabolites were identified, mainly involving ketoreduction, pyrrolidinyl oxidation, and N-dealkylation to *N*-butanoic acid or *N*-hydroxy-4′-ketobutyl [18]. Reduction of the ketone group is a prominent transformation in SC metabolism [19–23], but it is not detected in human liver microsomes and human S9 fractions [24–26]. In vitro incubations with human hepatocytes have proved suitable for the prediction of NPS metabolic fate in previous studies [27–34]. Additionally, it has proven particularly accurate for the prediction of urinary metabolites of structural analogues α-pyrrolidinoheptaphenone (PV8) and α-pyrrolidinopentiothiophenone (α-PVT) (Figure 1), suggesting an important hepatic metabolism of pyrrolidinyl SCs [21,22]. Combining human hepatocyte incubations and the analysis of urine samples from authentic users seems therefore the best strategy to identify optimal SC use markers. Considering the potential health threat of α-PHP and 4F-α-PVP, we investigated their metabolite fate using pooled human hepatocyte incubations, liquid chromatography–high-resolution tandem mass spectrometry (LC-HRMS/MS), and data-mining software, with the aim of identifying suitable markers of consumption.

2. Results and Discussion

2.1. α-PHP and 4F-α-PVP MS/MS Fragmentation Patterns

As expected from two structural analogues, α-PHP and 4F-α-PVP display similar fragmentation patterns (Figures 2 and 3). Major fragments are produced through C-C cleavage at the α carbons of the carbonyl and pyrrolidinyl groups, yielding fragments m/z 105.0334 and 140.1432 from α-PHP, and m/z 123.0241 and 126.1277 from 4F-α-PVP. Further fragmentation and rearrangement yield the characteristic tropylium ion from α-PHP (m/z 91.0542), the fluorotropylium ion from 4F-α-PVP (m/z 109.0448), and the pyridinium ion from both molecules (m/z 84.0808). C-C cleavage at the pyrrolidinyl α carbon also produces fragments m/z 175.1117 and 189.1147 for α-PHP, m/z 179.0867 and 207.1052 for 4F-α-PVP, and m/z 72.0808 for both. Further fragmentation produces fragments m/z 119.0491 and 137.0397 from fragments m/z 175.1117 and 179.0867, respectively. McLafferty rearrangement through the ionization of the oxygen atom may occur, yielding fragment m/z 70.0652 from α-PHP and 4F-α-PVP. α-PHP fragmentation matches well with that reported by Matsuta et al., although the instrument employed was different [35]. 4F-α-PVP MS/MS fragmentation was described by Uchiyama et al. by gas chromatography (GC)-MS, but the authors only identified two fragments, i.e., m/z 95 (attributed to the fluorophenyl group) and 126 [5].

2.2. α-PHP Metabolism with Human Hepatocytes

The α-PHP signal decreased to 21% after 3 h incubation with hepatocytes, generating a total of 24 metabolites. Five metabolites totaling more than 95% of the total metabolite peak area are described in this article are listed from P1 to P5 by ascending retention time (Figure 4). All metabolites were absent from controls, ruling out interferences and non-enzymatic reactions.
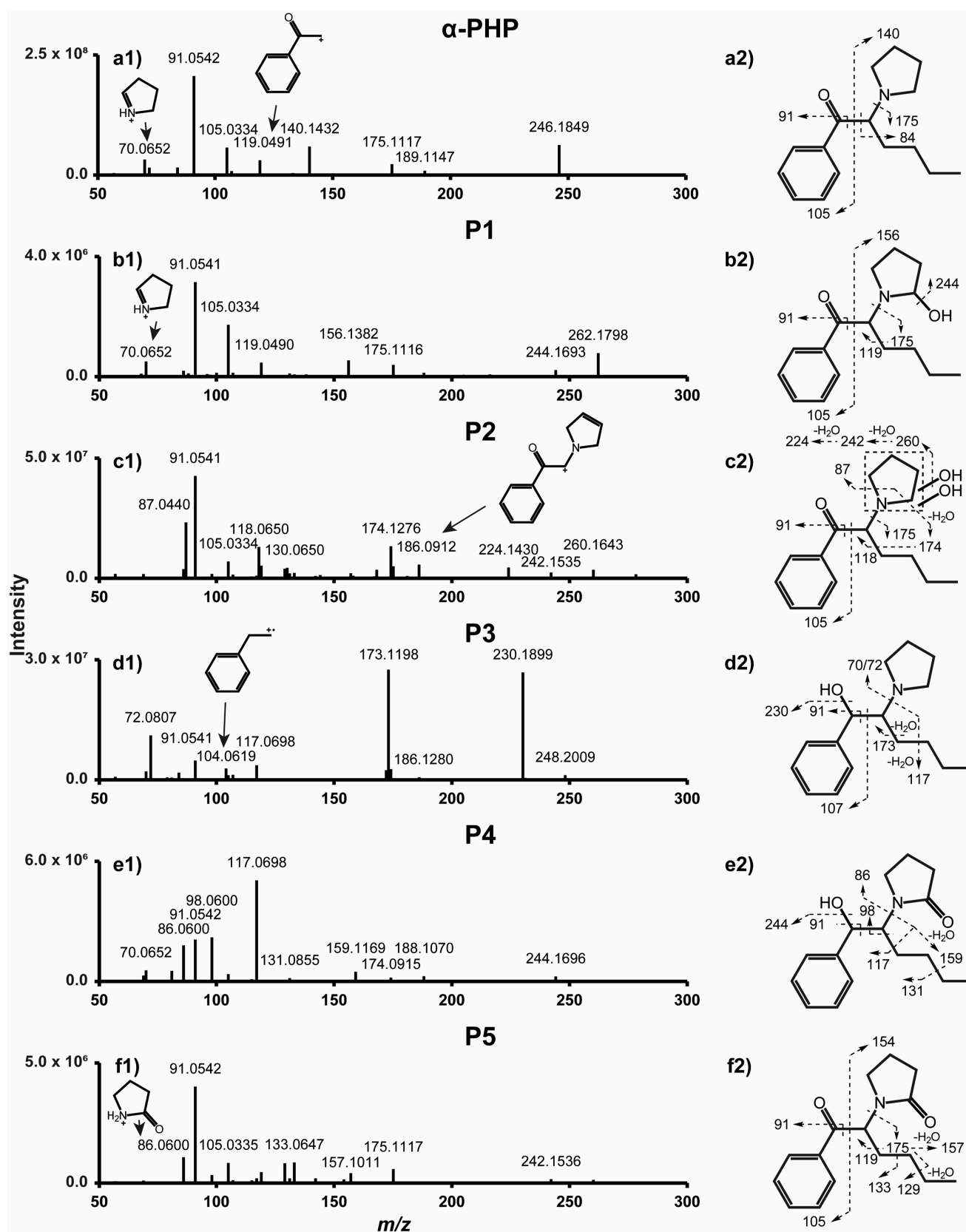
Figure 2. Product ion spectra of α-PHP (**a1**) and metabolites P1 (**b1**), P2 (**c1**), P3 (**d1**), P4 (**e1**), and P5 (**f1**), and their postulated fragmentation patterns (**a2–f2**, respectively). Dashed arrow indicates fragmentation site.
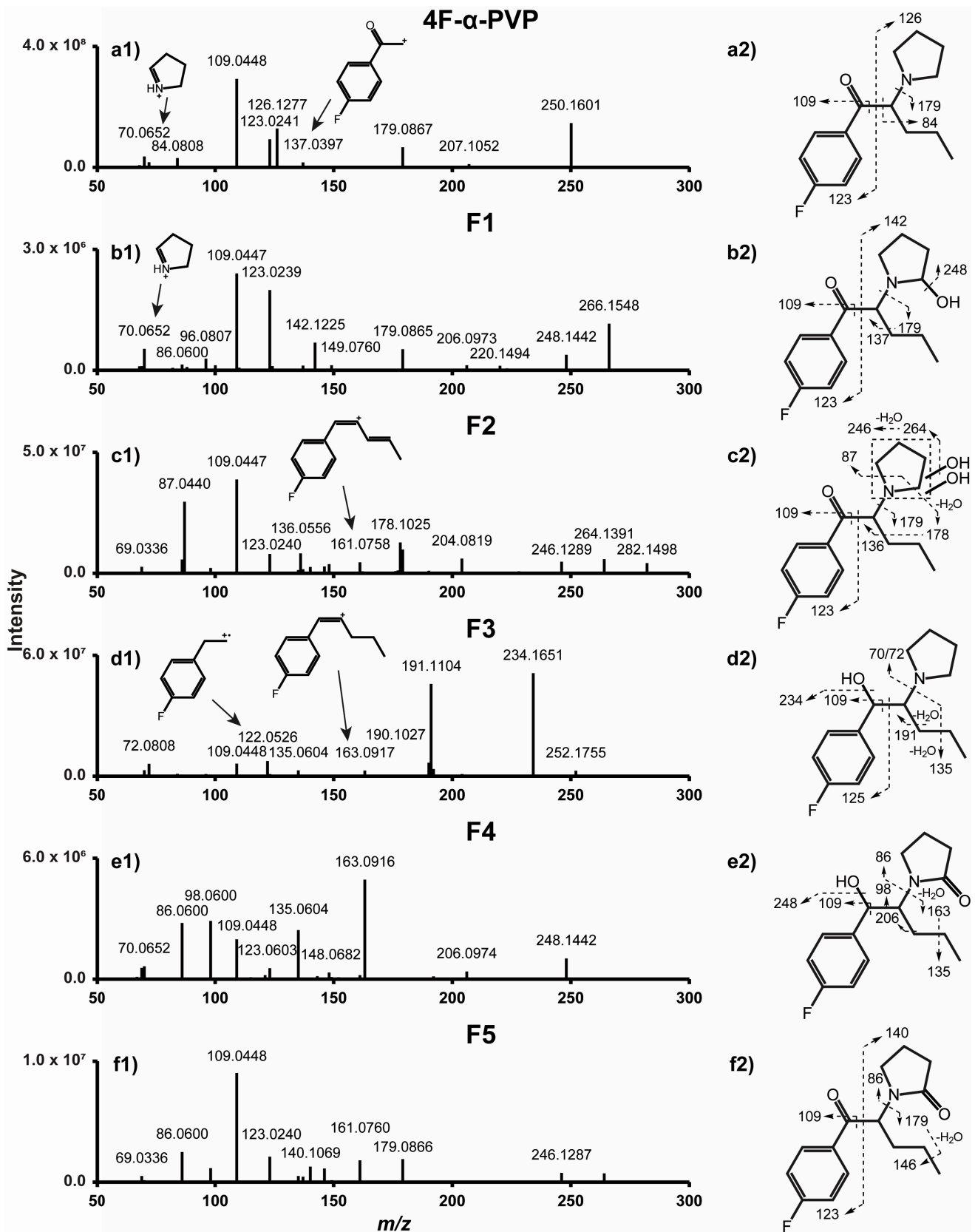
Figure 3. Product ion spectra of 4F-α-PVP (**a1**) and metabolites F1 (**b1**), F2 (**c1**), F3 (**d1**), F4 (**e1**), and F5 (**f1**), and their postulated fragmentation patterns (**a2–f2**, respectively). Dashed arrow indicates fragmentation site.
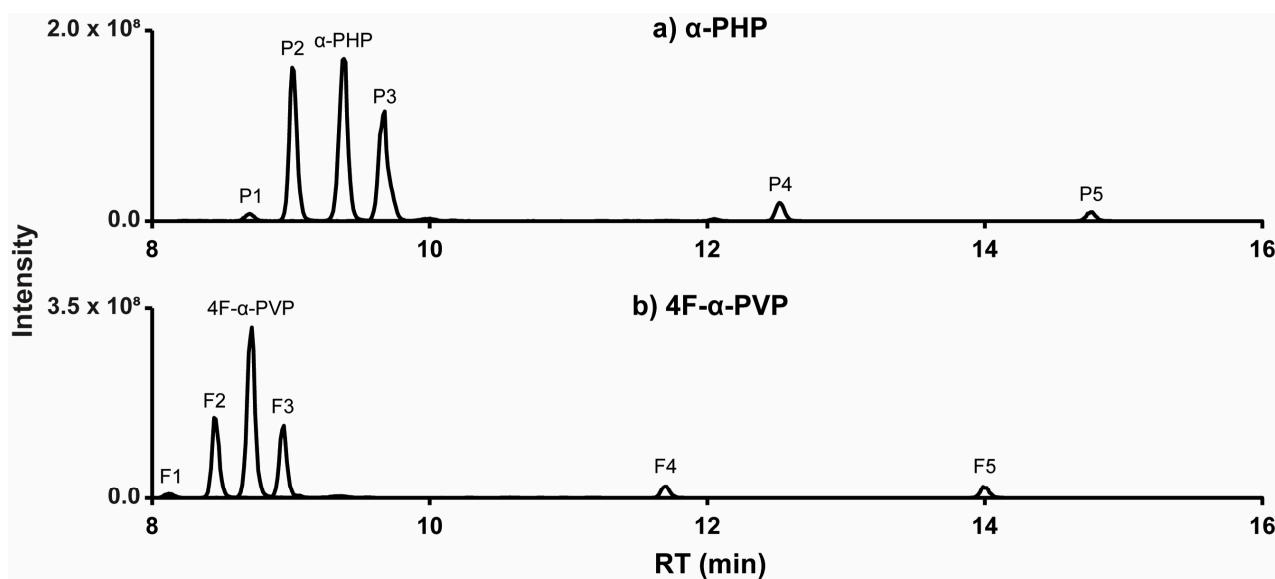
Figure 4. Combined extracted ion chromatogram of α-PHP (**a**), 4F-α-PVP (**b**), and metabolites obtained from 3 h hepatocyte incubation. Mass tolerance, 5 ppm; RT, retention time.

Major metabolic reactions included reduction of the ketone group (P3 and P4) and hydroxylation (P1 and P2) and oxidation (P4 and P5) of the pyrrolidinyl ring. Dealkylation to the primary amine and alkyl hydroxylation were identified as minor phase I metabolites. α-PHP alkyl chain transformations were less frequent than those of structural analogues with a longer chain [20,21]. However, Manier et al. reported that α-PHP was mainly hydroxylated at the pyrrolidinyl ring [26], in accordance with our results. In fact, the length of the alkyl chain seems to strongly influence the metabolic pathway of analogues [35]. Phase II glucuronidations were also rare, as observed in the metabolic profile of analogues (in vitro and in vivo) [21,22] and that of α-PHP in the urine of several users [18]. Therefore, hydrolysis may be not a prerequisite for the detection of α-PHP and metabolites in urine. The accurate mass molecular ion, retention time, elemental composition, nominal mass for diagnostic product ions, and mass spectrometry peak areas (extracted ion chromatogram) for P1–P5 are reported in Table 1. The fragmentation pattern of P1–P5 is displayed in Figure 2. α-PHP's metabolic pathway is proposed in Figure 5.

2.2.1. β-Ketoreduction

Reduction of the α-PHP ketone group (+2H) resulted in the formation of P3 (α-PHP hexanol), as suggested by a +2.0157 Da mass shift from parent and a water loss (*m/z* 230.1899) detected in P3's product-ion spectrum. The signal intensity of the water loss was particularly intense, as it is favored by the proximity of the phenyl group. The low intensity of ion *m/z* 70.0652 compared to *m/z* 72.0807), and the absence of ion *m/z* 177.1274 (*m/z* 175.1117 in α-PHP) suggested that McLafferty rearrangement did not occur, due to the reduction of the ketone group. Instead, ion *m/z* 173.1198, produced by C-C cleavage at the α carbon of the pyrrolidinyl group and a water loss, was intense. The presence of the tropylium ion further indicated that the phenyl group did not carry the transformation. β-ketoreduction is a prominent transformation in SC metabolism [19–23], and P3 was indeed one of the metabolites with the most intense signal in our experiments. It was also detected as a major metabolite by Paul et al. and Matsuta et al. in urine samples from α-PHP users [18,35].

Table 1. Accurate mass molecular ion, retention time (RT), elemental composition, nominal mass for diagnostic product ions, MS peak areas, and α-PHP and 4F-α-PVP metabolites peak area fraction (sum = 95 and 98%, respectively) in hepatocyte incubations. Peak area for α-PHP and 4F-α-PVP at T_{0h} were 6.1×10^7 and 7.5×10^7, respectively. Metabolites are listed by ascending RT. MS, mass spectrometry; ND, not detected.

ID	Biotransformation	$[M + H]^+$ (*m/z*)	RT (min)	Mass Error (ppm)	Elemental Composition	Diagnostic Product Ions (*m/z*)	Peak Area at T_{3h}	Metabolites Peak Area Fraction (%)
α-PHP	Parent drug	246.1848	9.38	1.79	$C_{16}H_{23}NO$	70, 91, 105, 119, 140, 175	1.3×10^7	
P1	Hydroxylation (α-PHP 2′-hydroxypyrrolidinyl)	262.1798	8.70	1.32	$C_{16}H_{23}NO_2$	70, 91, 105, 119, 156, 175	6.1×10^5	2.6%
P2	Dihydroxylation (α-PHP dihydroxy-pyrrolidinyl)	278.1746	9.02	1.72	$C_{16}H_{23}NO_3$	87, 91, 105, 118, 174, 186	1.0×10^7	44%
P3	β-Ketoreduction (α-PHP hexanol)	248.2005	9.66	1.63	$C_{16}H_{25}NO$	72, 91, 104, 117, 173, 230	9.7×10^6	40%
P4	β-Ketoreduction + Ketone formation (α-PHP 2′-ketopyrrolidinyl-hexanol)	262.1799	12.52	0.97	$C_{16}H_{23}NO_2$	70, 86, 91, 98, 117, 159	1.3×10^6	5.3%
P5	Ketone formation (α-PHP 2′-ketopyrrolidinyl)	260.1642	14.77	1.00	$C_{16}H_{21}NO_2$	86, 91, 105, 129, 133, 175	7.0×10^5	2.9%
4F-α-PVP	Parent drug	250.1598	8.71	1.33	$C_{15}H_{20}FNO$	70, 84, 109, 123, 126, 179	2.2×10^7	
F1	Hydroxylation (4F-α-PVP 2′-hydroxypyrrolidinyl)	266.1547	8.12	1.35	$C_{15}H_{20}FNO_2$	70, 109, 123, 142, 179, 248	6.4×10^5	2.8%
F2	Dihydroxylation (4F-α-PVP dihydroxy-pyrrolidinyl)	282.1496	8.46	1.42	$C_{15}H_{20}FNO_3$	87, 109, 123, 136, 178, 179	9.4×10^6	41%
F3	β-Ketoreduction (4F-α-PVP hexanol)	252.1755	8.94	1.18	$C_{15}H_{22}FNO$	72, 109, 122, 190, 191, 234	9.1×10^6	40%
F4	β-Ketoreduction + Ketone formation (4F-α-PVP 2′-ketopyrrolidinyl-hexanol)	266.1548	11.70	1.01	$C_{15}H_{20}FNO_2$	86, 98, 109, 135, 163, 248	1.7×10^6	7.4%
F5	Ketone formation (4F-α-PVP 2′-ketopyrrolidinyl)	264.1391	14.00	1.15	$C_{15}H_{18}FNO_2$	98, 109, 123, 140, 161, 179	1.6×10^6	7.1%
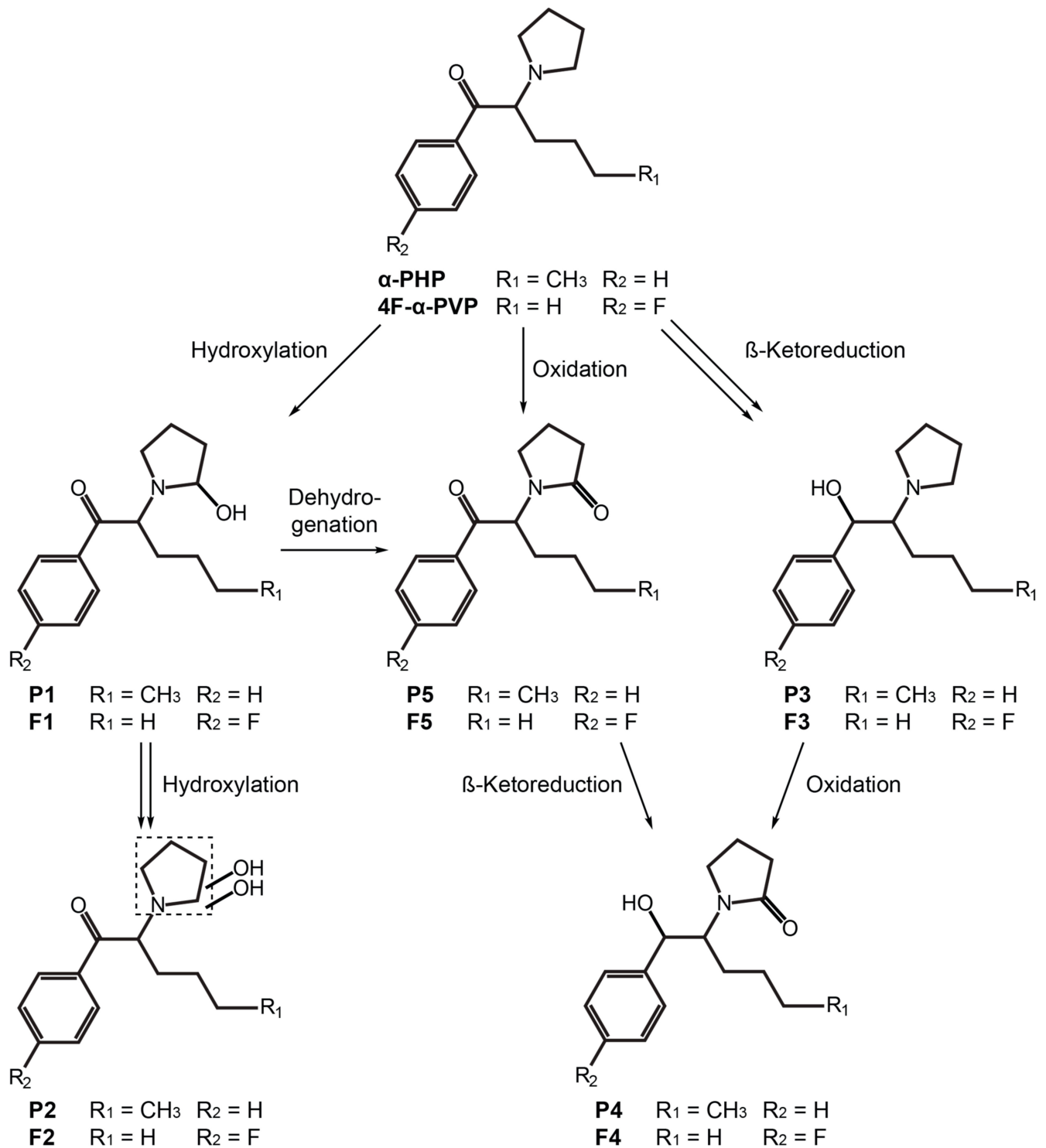
Figure 5. Postulated metabolic pathway of α-PHP and 4F-α-PVP. Double arrow indicates major pathway.

Reduction of the ketone group implies the formation of a chiral center and two diastereoisomers, depending on hydroxyl positioning. Matsuta et al. determined that the formation of one isomer is favored over the other (ten-times higher concentration), but they could not distinguish the two molecules [35]. Most probably, the two metabolites coeluted in our experiments, which is not problematic considering that HRMS/MS is not suitable to identify the two isomers.

2.2.2. Pyrrolidinyl Hydroxylation

P1 (α-PHP 2′-hydroxy-pyrrolidinyl) was formed by hydroxylation (+O), as suggested by a +15.9950 Da mass shift from the parents and a water loss (m/z 244.1693) detected after fragmentation. The presence of ions m/z 91.0542, 105.0335, and 175.1117, also detected in the α-PHP product-ion spectrum, indicated that the transformation occurred at the pyrrolidinyl ring. Ion m/z 156.1382 (m/z 140.1432 in α-PHP) also suggested that the hydroxylation occurred either at the pyrrolidinyl ring or the alkyl chain of the molecule. The exact position of the hydroxylation could not be determined. However, the metabolic profile of structural analogues α-PVP and α-PBP strongly suggests that the hydroxylation may have occurred at position 2′ of the pyrrolidinyl ring, forming a hemiaminal group that can be an intermediate to P4 and P5 (Section 2.2.3.) [36–38].

P2 (α-PHP dihydroxy-pyrrolidinyl) was the metabolite with the most intense signal detected in our experiments. The +31.9898 Da mass shift from α-PHP and the two water losses (m/z 260.1643 and 242.1535) suggested a dihydroxylation (+2O). Like P1, ions m/z 91.0541, 105.0334, and 175.1117 indicated that the transformations occurred at the pyrrolidinyl ring. Pyrrolidinyl dihydroxylation was also a major transformation in the metabolic pathway of 4-methoxy-α-PVP and α-PVT, two structural analogues, using human hepatocytes and urine samples from users [22,23]. P2's molecular mass and theoretical formula also match those of α-PHP *N*-butanoic acid, which could theoretically be formed by γ-lactam formation, then N-dealkylation and further carboxylation of the pyrrolidinyl ring, as reported in the metabolism of SCs with an analogous structure [26]. However, the absence of carboxylic acid loss and the presence of two water losses in the P2 fragmentation pattern rather indicate a dihydroxylation. Additionally, Vickers and Polsky determined that further transformation following lactam formation (Section 2.2.3.) is unlikely in the metabolism of N-heterocycles [36]. Lactam opening was observed in the metabolism of nicotine, an extensively studied molecule with a pyrrolidinyl substructure, but it was only a minor metabolic pathway [39]. Paul et al. identified two major α-PHP metabolites with P2 molecular mass in the urine of an authentic user, which they attributed to the formation of *N*-butanoic acid and *N*-hydroxy-4′-oxobutane (M13 or M14, respectively, in the article), both formed by lactam formation and opening of the N-heterocycle [18]. They correctly located the position of the transformations on the pyrrolidinyl ring of the molecule (fragments m/z 91.0542 and 175.1117). Like P2 in our experiments, the authors did not detect a carboxylic acid loss in the M13 and M14 fragmentation patterns, but they detected one (M13) or two (M14) water losses instead. They also detected further minor metabolites with subsequent hydroxylation and dealkylation. We believe that these data rather point towards two different dihydroxylations at the pyrrolidinyl ring, as identified in the present study (P2). Comparison with suitable analytical standards, which are yet to be synthesized, would bring a definite answer. In another article, Matsuta et al. did not identify P1 and P2 during their investigation of α-PHP metabolism using the urine of five authentic users, as they mainly focused on the metabolic transformations at the alkyl chain [35]. The characterization of P2, a potential major metabolite that was not reported in previous studies, might be crucial for documenting α-PHP use.

Manier et al. determined the kinetics of α-PHP hydroxylations using human liver microsomes and S9 human fractions [26]. They determined that cytochrome P450 (CYP) 2C9 is mainly involved in the hydroxylation of α-PHP (71% of reactions with selected enzymes); CYP2C19, CYP3A4, and CYP2B6 catalyzed 18%, 6%, and 5% of reactions, respectively.

2.2.3. Oxidation

Pyrrolidinyl oxidation or hydroxylation and dehydrogenation (+O −2H) occurred in P5 (α-PHP 2′-keto-pyrrolidinyl), as indicated by a +13.9794 Da mass shift from the parents and the detection of α-PHP fragments m/z 91.0542, 105.0335, and 175.1117. P5's late elution compared to parents supported an oxidation at position 2′ of the pyrrolidinyl ring (γ-lactam), which acts as a hindrance for hydrogen bonding [22]. In addition, 2′-pyrrolidinyl oxidation is another transformation that is predominant in the metabolism pyrrolidinyl-

containing molecules through CYP metabolism [36] and pyrrolidinyl SCs [19–24,26], and it was also detected as a major metabolite by Paul et al. and Matsuta et al. in urine samples from α-PHP users [18,35]. Fragment m/z 86.0600 may also be explained by another McLafferty rearrangement through the ionization of the newly formed amide group.

Following the same reasoning, we found that P4 (α-PHP 2′-keto-pyrrolidinyl-hexanol) was formed by oxidation at the pyrrolidinyl ring (+O –2H), as observed in P5, and a β-ketoreduction (+2H), as observed in P3 (Section 2.2.1.).

2.3. 4F-α-PVP Metabolism with Human Hepatocytes

The 4F-α-PVP signal decreased to 29% after 3 h incubation with human hepatocytes. A total of 11 metabolites were identified, with five molecules totaling more than 97% of the total metabolite peak area, which were listed from F1 to F5 by ascending retention time (Figure 4). All metabolites were absent in controls.

4F-α-PVP's major transformations were the same as those of α-PHP, with similar relative intensities (Table 1). Fewer minor metabolic reactions were detected, and no transformations of the alkyl chain were identified, in consistency with the results of Matsuta et al. on the influence of the alkyl chain length on the metabolic profile of analogues [35]. Several alkyl chain transformations, however, were observed in α-PVP metabolism using human hepatic microsomes and controlled administrations to rats [24]. No phase II transformations were detected either. The fragmentation pattern of F1–F5 is displayed in Figure 3. 4F-α-PVP's metabolic pathway is proposed in Figure 5.

2.3.1. β-Ketoreduction

Unsurprisingly, β-ketoreduction (+2H) appeared as a major metabolic transformation in our experiments, leading to F3 formation (4F-α-PVP hexanol). F3 fragmentation and fragment relative intensities were very similar to those of P3 (Section 2.2.1.), with fragment mass shifts depending on the fluorine atom and the alkyl side chain. Like α-PHP, mass shift from parent (+2.0157 Da), and ions m/z 72.0808, 109.0448, 191.1104, and 234.1651 allowed for F3 identification. β-ketoreduction is also a major metabolic transformation of α-PHP (Section 2.2.1.) and other SCs such as α-PBP, α-PVP, and α-PVT [19–23].

2.3.2. Pyrrolidinyl Hydroxylation

Pyrrolidinyl hydroxylation (+O) also occurred in 4F-α-PVP, producing F1 (4F-α-PVP 2′-hydroxy-pyrrolidinyl). Like F3, F1's fragmentation pattern and fragment relative intensities were similar to those of P1 (Section 2.2.2.). The mass shift from parents (+15.9949 Da) and ions m/z 109.0447, 123.0239, 142.1225, 179.0865, and 248.1442 indicated a hydroxylation at the pyrrolidinyl ring. As suggested by the metabolic profile of structural analogues α-PVP and α-PBP, the reaction probably occurred at position 2′ of the pyrrolidinyl ring, forming a hemiaminal group that can be an intermediate for F4 and F5 formation (Section 2.3.3.) [37,38].

Like α-PHP and other SCs [22,23], pyrrolidinyl dihydroxylation (+2O) was a major 4F-α-PVP metabolic transformation. F2 (4F-α-PVP dihydroxy-pyrrolidinyl) was identified through the +31.9898 Da mass shift from the parents and ions m/z 109.0447, 123.0240, and 179.0867, similar to α-PHP (Section 2.2.2.). Although the opening and carboxylation of the pyrrolidinyl ring was observed in the metabolism of several SCs with a similar structure [26], the absence of carboxylic acid and the presence of two water losses (m/z 264.1391 and 246.1289) in the F2 fragmentation pattern indicated a dihydroxylation.

2.3.3. Oxidation

Another frequent metabolic transformation of pyrrolidinyl SCs is the formation of a γ-lactam [19–24,26]. The F5 (4F-α-PVP 2′-keto-pyrrolidinyl) retention time shift and the +13.9793 Da mass shift from 4F-α-PVP, and ions m/z 109.0448, 123.0240, and 179.0866 indicated a formation of a ketone at position 2′ of the pyrrolidinyl ring, similar to α-PHP (Section 2.2.3.).

F4 (4F-α-PVP 2′keto-pyrrolidinyl-hexanol) was a combination of β-ketoreduction (+2H) and pyrrolidinyl oxidation (+O −2H).

2.4. Optimal Targets for α-PHP and 4F-α-PVP

The four α-PHP metabolites with the most intense signal intensity detected after 3 h incubation with human hepatocytes were α-PHP dihydroxy-pyrrolidinyl (P2), α-PHP hexanol (P3), α-PHP 2′-keto-pyrrolidinyl-hexanol (P4), and α-PHP 2′-keto-pyrrolidinyl (P5), with P2 and P3 representing almost 85% of the total metabolite peak area. Similarly, the four 4F-α-PVP metabolites with the most intense signal intensity were 4F-α-PVP dihydroxy-pyrrolidinyl (F2), 4F-α-PVP hexanol (F3), 4F-α-PVP 2′-keto-pyrrolidinyl-hexanol (F4), and 4F-α-PVP 2′-keto-pyrrolidinyl (F5), with F2 and F3 representing more than 80% of the total metabolite peak area. To the best of the authors' knowledge, these metabolites were not observed in the metabolism of other SCs and can be used as targets for α-PHP and 4F-α-PVP use. α-PiHP is an α-PHP isomer with a 4-methyl-pentanone structure instead of a hexanone, which was recently identified in seized materials [40]. α-PiHP possesses the same molecular formula and mass as those of α-PHP and the identification of the two SCs could be problematic. Although the metabolic fate of α-PiHP has not yet been studied, the alkyl chain of α-PHP major metabolites remained untransformed, and it is unlikely to observe P2, P3, P4, or P5 in α-PiHP metabolism. Similarly, α-PHP major metabolites are unlikely to be found in the metabolism of pyrovalerone, another isomer [41].

Glucuronide and sulfate hydrolysis are not required for PHP and 4F-α-PVP urinalysis due to the low incidence of phase II transformations.

2.5. Analytical Considerations

GC separation should be avoided for SC testing and metabolite identification, considering their thermal degradation through oxidative decomposition [42]. This decomposition was also observed with α-PVP, most likely resulting in formation of an enamine [43]. Although derivatization can increase SC thermal stability, pyrrolidinyl SCs are not derivatized with common reagents, and the derivatization of metabolites is not guaranteed [42]. Additionally, small molecules and metabolites may be unstable at high temperatures during derivatization or GC testing [44]. LC-MS/MS is typically used for metabolite identification studies, and HRMS is popular for identifying expected and unexpected metabolites with accurate-mass capabilities. We employed a long chromatographic run to best separate isomers and limit matrix effects. We selected a polar end-capped C_{18} column and a mobile phase gradient, as previously reported in other SC metabolite identification studies [21–23]. The lack of a buffer limited interference and ammonium, sodium, and potassium adducts. Metabolites are generally more polar than parent drugs to favor elimination. However, SC metabolites with γ-lactam formation often appeared to elute later than parents in reversed-phase chromatography [18,21–23,35]. Therefore, we ensured that αPHP and 4F-α-PVP approximately eluted mid-gradient to best separate the metabolites.

MS source parameters were optimized using α-PHP and 4F-α-PVP reference standards in an attempt to achieve good signals. However, the behavior of metabolites in these conditions is hardly predictable. Similarly, a ramped collision energy generated many specific fragments to allow metabolite identification, but optimal collision energy may differ from one metabolite to another. Two different injections with a different acquisition mode maximized the fragmentation of metabolites (Section 3.4.2.). Data-dependent MS/MS acquisition with dynamic exclusion and apex triggering enabled us to obtain a few MS/MS spectra for each chromatographic peak and allowed molecules with a less intense signal intensity to also trigger MS/MS spectra.

3. Material and Methods

3.1. Chemicals and Reagents

α-PHP (1-phenyl-2-(1′-pyrrolidinyl)-1-hexanone) and 4F-α-PVP (1-(4′′-fluorophenyl)-2-(1′-pyrrolidinyl)-1-pentanone) standards were purchased from Cayman Chemical (Ann

Arbor, MI, USA), and diclofenac standard was acquired from Toronto Research Chemicals (Toronto, ON, Canada). All the standards were dissolved in methanol to 1 mg/mL and stored at −20 °C until analysis. Water, formic acid, and methanol (Optima™ LC/MS) were from Fisher Scientific (Fair Lawn, NJ, USA), and acetonitrile was obtained from Sigma-Aldrich® (St. Louis, MO, USA). All the solvents and reagents were LC-MS grade. Ten-donor-pooled cryopreserved human hepatocytes and Krebs–Henseleit buffer (KHB) were purchased from BioreclamationIVT (Baltimore, MD, USA).

3.2. Incubation with Pooled Human Hepatocytes

Incubations with human hepatocytes were conducted following our on-site workflow, as previously described [45,46]. Briefly, the hepatocytes were thawed at 37 °C and solubilized in KHB to 2×10^6 viable cells/mL. Two hundred fifty microliters cell suspension was gently mixed with 250 μL of 20 μmol/L α-PHP or 4F-α-PVP in KHB and incubated at 37 °C for 0 or 3 h. Reactions were quenched with 500 μL acetonitrile and incubates were stored at −80 °C until analysis. Diclofenac was incubated under the same conditions to ensure proper metabolic activity. Negative controls with α-PHP or 4F-α-PVP in KHB without hepatocytes, and with KHB and hepatocytes without the drugs were incubated simultaneously. Each incubation was performed once due to the high cost of pooled human hepatocytes, but positive and negative controls were included to document appropriate metabolic activity and control for potential interference and contribution from the blank. The advantages and limitations of this approach are further discussed in two recent review articles [47,48].

3.3. Sample Preparation

Incubates were thawed at room temperature and vortex mixed. One hundred microliters was vortex mixed with 100 μL acetonitrile and centrifuged at 4 °C, $15,000 \times g$, for 10 min. Supernatants were evaporated to dryness at 40 °C, and the residues were reconstituted in 150 μL LC mobile phases A:B 80:20 (*v/v*). After centrifugation at 4 °C, $15,000 \times g$, for 5 min, supernatants were transferred into LC autosampler vials with glass inserts.

3.4. LC-HRMS/MS Parameters

LC-HRMS/MS analysis was performed on a Dionex Ultimate™ 3000 chromatography system coupled with a Thermo Scientific Q Exactive™ (Fremont, CA, USA) Plus mass spectrometer with a heated electrospray ionization (ESI) interface operating in positive-ion mode. During method optimization, α-PHP and 4F-α-PVP did not produce any signal when ESI was operated in negative-ion mode, and their metabolites were likely to produce a signal in positive-ion mode. Data reprocessing was performed in Ancona, Italy, on a Dionex Ultimate™ 3000 coupled with a Q Exactive™ (Ancona, Italy) combined with heated ESI operating in the same conditions.

3.4.1. LC Parameters

Samples were kept at 15 °C in an autosampler and 15 μL was injected onto the chromatographic system. Separation was achieved on a Synergi™ Hydro-RP column (100 × 2.0 mm, 4.0 μm; Phenomenex, Torrance, CA, USA) equipped with a guard cartridge of identical stationary phase (10 × 2.1 mm; Phenomenex) that was maintained at 30 °C throughout the analysis. A 30 min elution was performed with 0.1% formic acid in water (mobile phase A) and 0.1% formic acid in acetonitrile (mobile phase B) at a 0.4 mL/min flow rate—the gradient started with 2% B held for 2 min, was increased to 95% B within 18 min, and was held at 95% B for 5 min, before returning to initial conditions within 1 min, followed by a 4-min equilibration. LC efflux was diverted to waste the first 2 min and the last 5 min of the gradient.

3.4.2. HRMS/MS Parameters

Source parameters were optimized by post-column infusion of α-PHP and 4F-α-PVP standards in LC mobile phases A:B 50:50 (*v/v*) at 0.5 mL/min. Source parameters for α-PHP incubates were: spray voltage, 4 kV; sheath gas flow rate, 50 arbitrary units (a.u.); auxiliary gas flow rate, 5 a.u.; sweep gas flow rate, 2 a.u.; S-lens radio frequency level, 50 a.u.; auxiliary gas heater temperature, 400 °C; capillary temperature, 300 °C. Source parameters for 4F-α-PVP incubates were: spray voltage, 4 kV; sheath gas flow rate, 40 a.u.; auxiliary gas flow rate, 5 a.u.; sweep gas flow rate, 2 a.u.; S-lens radio frequency level, 50 a.u.; auxiliary gas heater temperature, 500 °C; capillary temperature, 300 °C. Injections were performed in duplicate with two different acquisition modes to obtain orthogonal spectral information.

In a first injection, data were acquired in full-scan MS (FullMS) and data-dependent MS/MS (ddMS^2) modes, which triggered MS/MS data acquisitions based on the intensity of the ions detected in FullMS scans and an inclusion list of expected metabolites. FullMS settings were: resolution, 70,000; scan time, 2–25 min; mass range, *m/z* 100–500; automatic gain control (AGC) target, 1×10^6; max injection time (IT), 200 ms. ddMS^2 settings were: resolution, 17,500; topN, 5 (pick others if idle); intensity threshold, 2×10^4; isolation window, *m/z* 1.5; normalized collision energy (NCE), 40%, 50%, and 60% (35%, 50%, and 65% for 4F-α-PVP); apex triggering, 3–6 s; dynamic exclusion, 2 s; AGC target, 1×10^5; max IT, 50 ms. Inclusion lists were generated based on prior metabolite identification studies [21–23,49] and postulation (Table 2).

Table 2. Inclusion and neutral loss lists for the FullMS/ddMS2 and FullMS/AIF/ddMS2 acquisitions, respectively, used during HRMS analysis of hepatocytes incubations. FullMS/ddMS2, full-scan mass spectrometry/data-dependent tandem mass spectrometry; FullMS/AIF/ddMS2, full-scan mass spectrometry/all-ion fragmentation/data-dependent tandem mass spectrometry; HRMS, high resolution mass spectrometry.

α-PHP.

FullMS/ddMS^2 acquisition					
[M + H]$^+$ (*m/z*)	**Formula**	**[M + H]$^+$ (*m/z*)**	**Formula**	**[M + H]$^+$ (*m/z*)**	**Formula**
192.1383	$C_{12}H_{17}NO$	260.1645	$C_{16}H_{21}NO_2$	280.1907	$C_{16}H_{25}NO_3$
208.1332	$C_{12}H_{17}NO_2$	262.1802	$C_{16}H_{23}NO_2$	292.1543	$C_{16}H_{21}NO_4$
244.1696	$C_{16}H_{21}NO$	264.1958	$C_{16}H_{25}NO_2$	296.1856	$C_{16}H_{25}NO_4$
246.1852	**$C_{16}H_{23}NO$**	276.1594	$C_{16}H_{21}NO_3$	342.1370	$C_{16}H_{23}NSO_5$
248.2009	$C_{16}H_{25}NO$	278.1751	$C_{16}H_{23}NO_3$	438.2122	$C_{22}H_{31}NO_8$

FullMS/AIF/ddMS^2 acquisition					
Neutral loss (*m/z*)	**Fragment loss**	**Neutral loss (*m/z*)**	**Fragment loss**	**Neutral loss (*m/z*)**	**Fragment loss**
−57.0704	−C_4H_9	−127.1361	−$C_8H_{17}N$	−174.1044	−$C_{12}H_{14}O$
−71.0735	−C_4H_9N	−141.1517	−$C_9H_{19}N$	−176.1201	−$C_{12}H_{16}O$
−79.9563	−SO_3	−155.1310	−$C_9H_{17}NO$	−176.0315	−$C_6H_8O_6$
−106.0418	−C_7H_6O	−162.1044	−$C_{11}H_{14}O$		

4F-α-PVP

FullMS/ddMS^2 acquisition					
[M + H]$^+$ (*m/z*)	**Formula**	**[M + H]$^+$ (*m/z*)**	**Formula**	**[M + H]$^+$ (*m/z*)**	**Formula**
194.1176	$C_{11}H_{15}NO_2$	252.1758	$C_{15}H_{22}FNO$	282.1700	$C_{15}H_{23}NO_4$
196.1132	$C_{11}H_{14}FNO$	262.1438	$C_{15}H_{19}NO_3$	284.1657	$C_{15}H_{22}FNO_3$
212.1081	$C_{11}H_{14}FNO_2$	264.1394	$C_{15}H_{18}FNO_2$	296.1293	$C_{15}H_{18}FNO_4$
232.1696	$C_{15}H_{21}NO$	264.1594	$C_{15}H_{21}NO_3$	300.1606	$C_{15}H_{22}FNO_4$
246.1489	$C_{15}H_{19}NO_2$	266.1551	$C_{15}H_{20}FNO_2$	328.1213	$C_{15}H_{21}NSO_5$
248.1445	$C_{15}H_{18}FNO$	268.1707	$C_{15}H_{22}FNO_2$	346.1119	$C_{15}H_{20}FNSO_5$
248.1645	$C_{15}H_{21}NO_2$	278.1387	$C_{15}H_{19}NO_4$	424.1966	$C_{21}H_{29}NO_8$
250.1602	**$C_{15}H_{20}FNO$**	280.1344	**$C_{15}H_{18}FNO_3$**	442.1872	$C_{21}H_{28}FNO_8$
250.1802	$C_{15}H_{23}NO_2$	282.1500	$C_{15}H_{20}FNO_3$		

Table 2. *Cont.*

FullMS/AIF/ddMS^2 acquisition					
Neutral loss (*m/z*)	Fragment loss	Neutral loss (*m/z*)	Fragment loss	Neutral loss (*m/z*)	Fragment loss
−43.0548	−C$_3$H$_7$	−124.0325	−C$_7$H$_5$FO	−176.0315	−C$_6$H$_8$O$_6$
−71.0735	−C$_4$H$_9$N	−127.1361	−C$_8$H$_{17}$N	−178.0794	−C$_{11}$H$_{11}$FO
−79.9563	−SO$_3$	−141.1154	−C$_8$H$_{15}$NO	−180.0951	−C$_{11}$H$_{13}$FO
−113.1205	−C$_7$H$_{15}$N	−166.0794	−C$_{10}$H$_{11}$FO		

Bold indicates parent drugs.

In a second injection, data were acquired in FullMS/all-ion fragmentation (AIF)/ddMS^2 mode, which triggered MS/MS data acquisitions based on specific neutral losses detected in FullMS and AIF scans. FullMS and ddMS^2 settings were the same as described above. Resolution, intensity threshold, mass range, NCE, AGC target, and max IT were the same as those of ddMS^2. Neutral loss lists were generated based on the fragmentation pattern of parent drugs, i.e., α-PHP or 4F-α-PVP, in the conditions of the analysis, and including glucuronide and sulfate losses in case of phase II metabolism (Table 2).

3.5. Metabolite Identification

Raw data files from 0 and 3 h incubations and controls were processed with Compound Discoverer™ (Thermo Scientific; Ancona, Italy) and compiled in a single analysis. Retention times of the chromatographic peaks were aligned following an adaptive curve model with a 5-ppm mass tolerance and a 0.1-min maximum time shift. Mass tolerance for MS identification was 5 ppm, with a 13,000 intensity threshold (20,000 for 4F-α-PVP) and a 50% intensity tolerance for isotopes. Mass tolerance for fragment identification was 10 ppm, with a signal-to-noise ratio higher than 3. Chromatographic peaks detected in controls with a similar or higher intensity than α-PHP and 4F-α-PVP incubations were filtered out. Detected peaks were compared to a list of theoretical molecules automatically generated by a combination of probable metabolic transformations, following the settings displayed in Table 3.

Table 3. Compound Discoverer™ processing settings for identifying α-PHP and 4F-α-PVP metabolites.

	α-PHP	4F-α-PVP
Phase I expected transformations	Dehydrogenation (–2H), dihydrodiol formation (+2O +2H), oxidation (+O), oxidative deamination to alcohol (–N +O –H), oxidative deamination to ketone (–N +O –3H), reduction (+2H)	Dehydrogenation (–2H), dihydrodiol formation (+2O +2H), oxidation (+O), oxidative deamination to alcohol (–N +O –H), oxidative deamination to ketone (–N +O –3H), oxidative defluorination (–F +O +H), reduction (+2H), reductive defluorination (–F +H)
Phase II expected transformations	Acetylation (+2C +O +2H), glucuronidation (+6C +6O +10H), sulfation (+S +3O)	Acetylation (+2C +O +2H), glucuronidation (+6C +6O +10H), sulfation (+S +3O)
Maximum number of dealkylation steps	2	2
Maximum number of phase II reactions	1	1
Maximum number of reactions	5	5

4. Conclusions

We have provided the first metabolic profile of 4F-α-PVP and identified an additional major metabolite of α-PHP using human hepatocyte incubations, LC-HRMS/MS analysis, and data-mining software. We suggest α-PHP dihydroxy-pyrrolidinyl (P2), α-PHP hexanol (P3), α-PHP 2′-keto-pyrrolidinyl-hexanol (P4), and α-PHP d2′-keto-pyrrolidinyl (P5) as markers of α-PHP use, and 4F-α-PVP dihydroxy-pyrrolidinyl (F2), 4F-α-PVP hexanol (F3), 4F-α-PVP 2′-keto-pyrrolidinyl-hexanol (F4), and 4F-α-PVP d2′-keto-pyrrolidinyl (F5) as markers of 4F-α-PVP use. The identification of this new α-PHP metabolite (P2) may be

critical to prove α-PHP use in clinical or forensic settings and to further substantiate findings from hepatic microsome investigations. These results must be confirmed with further experiments using suitable reference standards. Additionally, these are also valuable data for standard manufacturers to focus their synthesis efforts. Further pharmacokinetic and pharmacodynamic studies should be performed to better understand the effects of α-PHP and 4F-α-PVP.

Author Contributions: Conceptualization, J.C., X.D., and M.A.H.; methodology, J.C. and X.D.; formal analysis, J.C. and X.D.; writing—original draft preparation, J.C.; writing—review and editing, X.D., R.G., F.P.B., and M.A.H.; supervision, R.G., F.P.B., and M.A.H.; funding acquisition, R.G., F.P.B., and M.A.H. All authors have read and agreed to the published version of the manuscript.

Institutional Review Board Statement: Not applicable.

Informed Consent Statement: Not applicable.

Data Availability Statement: Data is contained within the article.

Conflicts of Interest: The authors declare no conflict of interest.

Abbreviations

SC	Synthetic cathinone
NPS	Novel psychoactive substance
DAT	Dopamine transporter
NET	Norepinephrine transporter
SERT	Serotonin transporter
MDMA	3″,4″-Methylenedioxymethamphetamine
MDPV	Methylenedioxypyrovalerone
α-PHP	α-pyrrolidinohexaphenone
4F-α-PVP	4″-Fluoro-α-pyrrolidinovalerophenone
α-PVP	α-Pyrrolidinovalerophenone
MDPH	3″,4″-Methylenedioxy-α-pyrrolidinohexiophenone
EMCDDA	European Monitoring Centre for Drugs and Drug Addiction
UNODC	United Nations Office on Drugs and Crime
WHO	World Health Organization
PV8	α-Pyrrolidinoheptaphenone
α-PVT	α-Pyrrolidinopentiothiophenone
LC	Liquid chromatography
MS	Mass spectrometry
MS/MS	Tandem mass spectrometry
HRMS	High resolution mass spectrometry
GC	Gas chromatography
FullMS	Full scan
ddMS^2	Data-dependent tandem mass spectrometry
AIF	All-ion fragmentation
AGC	Automatic gain control
IT	Injection time

References

1. Zaami, S.; Giorgetti, R.; Pichini, S.; Pantano, F.; Marinelli, E.; Busardò, F.P. Synthetic cathinones related fatalities: An update. *Eur. Rev. Med. Pharmacol. Sci.* **2018**, *22*, 268–274. [CrossRef] [PubMed]
2. La Maida, N.; Di Trana, A.; Giorgetti, R.; Tagliabracci, A.; Busardò, F.P.; Huestis, M.A. A review of synthetic cathinone-related fatalities from 2017 to 2020. *Ther. Drug Monit.* **2020**. [CrossRef] [PubMed]
3. Luethi, D.; Liechti, M.E. Designer drugs: Mechanism of action and adverse effects. *Arch. Toxicol.* **2020**, *94*, 1085–1133. [CrossRef] [PubMed]

4. Uchiyama, N.; Shimokawa, Y.; Kawamura, M.; Kikura-Hanajiri, R.; Hakamatsuka, T. Chemical analysis of a benzofuran derivative, 2-(2-ethylaminopropyl)benzofuran (2-EAPB), eight synthetic cannabinoids, five cathinone derivatives, and five other designer drugs newly detected in illegal products. *Forensic Toxicol.* **2014**, *32*, 266–281. [CrossRef]

5. Uchiyama, N.; Matsuda, S.; Kawamura, M.; Shimokawa, Y.; Kikura-Hanajiri, R.; Aritake, K.; Urade, Y.; Goda, Y. Characterization of four new designer drugs, 5-chloro-NNEI, NNEI indazole analog, α-PHPP and α-POP, with 11 newly distributed designer drugs in illegal products. *Forensic Sci. Int.* **2014**, *243*, 1–13. [CrossRef]

6. Fels, H.; Lottner-Nau, S.; Sax, T.; Roider, G.; Graw, M.; Auwärter, V.; Musshoff, F. Postmortem concentrations of the synthetic opioid U-47700 in 26 fatalities associated with the drug. *Forensic Sci. Int.* **2019**, *301*, e20–e28. [CrossRef]

7. Adamowicz, P.; Hydzik, P. Fetal death associated with the use of 3,4-MDPHP and α-PHP. *Clin. Toxicol.* **2019**, *57*, 112–116. [CrossRef]

8. Freni, F.; Bianco, S.; Vignali, C.; Groppi, A.; Moretti, M.; Osculati, A.M.M.; Morini, L. A multi-analyte LC–MS/MS method for screening and quantification of 16 synthetic cathinones in hair: Application to postmortem cases. *Forensic Sci. Int.* **2019**, *298*, 115–120. [CrossRef]

9. Vignali, C.; Moretti, M.; Groppi, A.; Osculati, A.M.M.; Tajana, L.; Morini, L. Distribution of the synthetic cathinone α-pyrrolidinohexiophenone in biological specimens. *J. Anal. Toxicol.* **2019**, *43*, e1–e6. [CrossRef]

10. Carlier, J.; La Maida, N.; Di Trana, A.; Huestis, M.A.; Pichini, S.; Busardò, F.P. Testing unconventional matrices to monitor for prenatal exposure to heroin, cocaine, amphetamines, synthetic cathinones, and synthetic opioids. *Ther. Drug Monit.* **2020**, *42*, 205–221. [CrossRef]

11. World Health Organization (WHO). *Critical Review Report: Alpha-PHP (α-Pyrrolidinohexanophenone) or PV-7*; WHO: Geneva, Switzerland, 2019.

12. Bonano, J.S.; Banks, M.L.; Kolanos, R.; Sakloth, F.; Barnier, M.L.; Glennon, R.A.; Cozzi, N.V.; Partilla, J.S.; Baumann, M.H.; Negus, S.S. Quantitative structure-activity relationship analysis of the pharmacology of para-substituted methcathinone analogues. *Br. J. Pharmacol.* **2015**, *172*, 2433–2444. [CrossRef] [PubMed]

13. Suyama, J.A.; Sakloth, F.; Kolanos, R.; Glennon, R.A.; Lazenka, M.F.; Negus, S.S.; Banks, M.L. Abuse-related neurochemical effects of para-substituted methcathinone analogs in rats: Microdialysis studies of nucleus accumbens dopamine and serotonin. *J. Pharmacol. Exp. Ther.* **2016**, *356*, 182–190. [CrossRef] [PubMed]

14. Eshleman, A.J.; Nagarajan, S.; Wolfrum, K.M.; Reed, J.F.; Swanson, T.L.; Nilsen, A.; Janowsky, A. Structure-activity relationships of bath salt components: Substituted cathinones and benzofurans at biogenic amine transporters. *Psychopharmacology* **2019**, *236*, 939–952. [CrossRef]

15. Luethi, D.; Walter, M.; Zhou, X.; Rudin, D.; Krähenbühl, S.; Liechti, M.E. Para-halogenation affects monoamine transporter inhibition properties and hepatocellular toxicity of amphetamines and methcathinones. *Front. Pharmacol.* **2019**, *10*, 438. [CrossRef] [PubMed]

16. World Health Organization (WHO). *World Health Organization Recommends 12 NPS for Scheduling*; WHO: Geneva, Switzerland, 2019.

17. National Institute of Health Sciences (NIHS). Data Search System for New Psychoactive Substances. Available online: https://npsdb.nihs.go.jp (accessed on 11 November 2020).

18. Paul, M.; Bleicher, S.; Guber, S.; Ippisch, J.; Polettini, A.; Schultis, W. Identification of phase i and II metabolites of the new designer drug α-pyrrolidinohexiophenone (α-PHP) in human urine by liquid chromatography quadrupole time-of-flight mass spectrometry (LC-QTOF-MS). *J. Mass Spectrom.* **2015**, *50*, 1305–1317. [CrossRef] [PubMed]

19. Matsuta, S.; Shima, N.; Kamata, H.; Kakehashi, H.; Nakano, S.; Sasaki, K.; Kamata, T.; Nishioka, H.; Miki, A.; Katagi, M.; et al. Metabolism of the designer drug α-pyrrolidinobutiophenone (α-PBP) in humans: Identification and quantification of the phase I metabolites in urine. *Forensic Sci. Int.* **2015**, *249*, 181–188. [CrossRef]

20. Shima, N.; Kakehashi, H.; Matsuta, S.; Kamata, H.; Nakano, S.; Sasaki, K.; Kamata, T.; Nishioka, H.; Zaitsu, K.; Sato, T.; et al. Urinary excretion and metabolism of the α-pyrrolidinophenone designer drug 1-phenyl-2-(pyrrolidin-1-yl)octan-1-one (PV9) in humans. *Forensic Toxicol.* **2015**, *33*, 279–294. [CrossRef]

21. Swortwood, M.J.; Ellefsen, K.N.; Wohlfarth, A.; Diao, X.; Concheiro-Guisan, M.; Kronstrand, R.; Huestis, M.A. First metabolic profile of PV8, a novel synthetic cathinone, in human hepatocytes and urine by high-resolution mass spectrometry. *Anal. Bioanal. Chem.* **2016**, *408*, 4845–4856. [CrossRef]

22. Swortwood, M.J.; Carlier, J.; Ellefsen, K.N.; Wohlfarth, A.; Diao, X.; Concheiro-Guisan, M.; Kronstrand, R.; Huestis, M.A. In vitro, in vivo and in silico metabolic profiling of α-pyrrolidinopentiothiophenone, a novel thiophene stimulant. *Bioanalysis* **2016**, *8*, 65–82. [CrossRef]

23. Ellefsen, K.N.; Wohlfarth, A.; Swortwood, M.J.; Diao, X.; Concheiro, M.; Huestis, M.A. 4-Methoxy-α-PVP: In silico prediction, metabolic stability, and metabolite identification by human hepatocyte incubation and high-resolution mass spectrometry. *Forensic Toxicol.* **2016**, *34*, 61–75. [CrossRef]

24. Sauer, C.; Peters, F.T.; Haas, C.; Meyer, M.R.; Fritschi, G.; Maurera, H.H. New designer drug α-pyrrolidinovalerophenone (PVP): Studies on itsmetabolism and toxicological detection in rat urine using gas chromatographic/mass spectrometric techniques. *J. Mass Spectrom.* **2009**, *44*, 952–964. [CrossRef] [PubMed]

25. Meyer, M.R.; Vollmar, C.; Schwaninger, A.E.; Wolf, E.U.; Maurer, H.H. New cathinone-derived designer drugs 3-bromomethcathinone and 3-fluoromethcathinone: Studies on their metabolism in rat urine and human liver microsomes using GC-MS and LC-high-resolution MS and their detectability in urine. *J. Mass Spectrom.* **2012**, *47*, 253–262. [CrossRef] [PubMed]
26. Manier, S.K.; Richter, L.H.J.; Schäper, J.; Maurer, H.H.; Meyer, M.R. Different in vitro and in vivo tools for elucidating the human metabolism of alpha-cathinone-derived drugs of abuse. *Drug Test. Anal.* **2018**. [CrossRef] [PubMed]
27. Wohlfarth, A.; Scheidweiler, K.B.; Pang, S.; Zhu, M.; Castaneto, M.; Kronstrand, R.; Huestis, M.A. Metabolic characterization of AH-7921, a synthetic opioid designer drug: In vitro metabolic stability assessment and metabolite identification, evaluation of in silico prediction, and in vivo confirmation. *Drug Test. Anal.* **2016**, *8*, 779–791. [CrossRef]
28. Diao, X.; Carlier, J.; Zhu, M.; Pang, S.; Kronstrand, R.; Scheidweiler, K.B.; Huestis, M.A. In vitro and in vivo human metabolism of a new synthetic cannabinoid NM-2201 (CBL-2201). *Forensic Toxicol.* **2017**, *35*, 20–32. [CrossRef]
29. Diao, X.; Carlier, J.; Scheidweiler, K.B.; Huestis, M.A. In vitro metabolism of new synthetic cannabinoid SDB-006 in human hepatocytes by high-resolution mass spectrometry. *Forensic Toxicol.* **2017**, *35*, 252–262. [CrossRef]
30. Carlier, J.; Diao, X.; Sempio, C.; Huestis, M.A. Identification of new synthetic cannabinoid ADB-CHMINACA (MAB-CHMINACA) metabolites in human hepatocytes. *AAPS J.* **2017**, *19*, 568–577. [CrossRef]
31. Wohlfarth, A.; Roman, M.; Andersson, M.; Kugelberg, F.C.; Diao, X.; Carlier, J.; Eriksson, C.; Wu, X.; Konradsson, P.; Josefsson, M.; et al. 25C-NBOMe and 25I-NBOMe metabolite studies in human hepatocytes, in vivo mouse and human urine with high-resolution mass spectrometry. *Drug Test. Anal.* **2017**, *9*, 680–698. [CrossRef]
32. Diao, X.; Carlier, J.; Zhu, M.; Huestis, M.A. Human hepatocyte metabolism of novel synthetic cannabinoids MN-18 and its 5-fluoro analog 5F-MN-18. *Clin. Chem.* **2017**, *63*, 1753–1763. [CrossRef]
33. Diao, X.; Carlier, J.; Zhu, M.; Huestis, M.A. Metabolism of the new synthetic cannabinoid EG-018 in human hepatocytes by high-resolution mass spectrometry. *Forensic Toxicol.* **2018**, *36*, 304–312. [CrossRef]
34. Carlier, J.; Diao, X.; Huestis, M.A. Synthetic cannabinoid BB-22 (QUCHIC): Human hepatocytes metabolism with liquid chromatography-high resolution mass spectrometry detection. *J. Pharm. Biomed. Anal.* **2018**, *157*, 27–35. [CrossRef] [PubMed]
35. Matsuta, S.; Shima, N.; Kakehashi, H.; Kamata, H.; Nakano, S.; Sasaki, K.; Kamata, T.; Nishioka, H.; Miki, A.; Zaitsu, K.; et al. Metabolism of α-PHP and α-PHPP in humans and the effects of alkyl chain lengths on the metabolism of α-pyrrolidinophenone-type designer drugs. *Forensic Toxicol.* **2018**, *36*, 486–497. [CrossRef] [PubMed]
36. Vickers, S.; Polsky, S. The biotransformation of nitrogen containing xenobiotics to lactams. *Curr. Drug Metab.* **2000**, *1*, 357–389. [CrossRef] [PubMed]
37. Shima, N.; Katagi, M.; Kamata, H.; Matsuta, S.; Sasaki, K.; Kamata, T.; Nishioka, H.; Miki, A.; Tatsuno, M.; Zaitsu, K.; et al. Metabolism of the newly encountered designer drug α-pyrrolidinovalerophenone in humans: Identification and quantitation of urinary metabolites. *Forensic Toxicol.* **2014**, *32*, 59–67. [CrossRef]
38. Grapp, M.; Sauer, C.; Vidal, C.; Müller, D. GC-MS analysis of the designer drug α-pyrrolidinovalerophenone and its metabolites in urine and blood in an acute poisoning case. *Forensic Sci. Int.* **2016**, *259*, e14–e19. [CrossRef]
39. Hukkanen, J.; Jacob, P.; Benowitz, N.L. Metabolism and disposition kinetics of nicotine. *Pharmacol. Rev.* **2005**, *57*, 79–115. [CrossRef]
40. Liu, C.; Jia, W.; Li, T.; Hua, Z.; Qian, Z. Identification and analytical characterization of nine synthetic cathinone derivatives N-ethylhexedrone, 4-Cl-pentedrone, 4-Cl-α-EAPP, propylone, N-ethylnorpentylone, 6-MeO-bk-MDMA, α-PiHP, 4-Cl-α-PHP, and 4-F-α-PHP. *Drug Test. Anal.* **2017**, *9*, 1162–1171. [CrossRef]
41. Michaelis, W.; Russel, J.H.; Schindler, O. The metabolism of pyrovalerone hydrochloride. *J. Med. Chem.* **1970**, *13*, 497–503. [CrossRef]
42. Kerrigan, S.; Savage, M.; Cavazos, C.; Bella, P. Thermal degradation of synthetic cathinones: Implications for forensic toxicology. *J. Anal. Toxicol.* **2016**, *40*, 1–11. [CrossRef]
43. Tsujikawa, K.; Kuwayama, K.; Kanamori, T.; Iwata, Y.T.; Inoue, H. Thermal degradation of α-pyrrolidinopentiophenone during injection in gas chromatography/mass spectrometry. *Forensic Sci. Int.* **2013**, *231*, 296–299. [CrossRef]
44. Fang, M.; Ivanisevic, J.; Benton, H.P.; Johnson, C.H.; Patti, G.J.; Hoang, L.T.; Uritboonthai, W.; Kurczy, M.E.; Siuzdak, G. Thermal degradation of small molecules: A global metabolomic investigation. *Anal. Chem.* **2015**, *87*, 10935–10941. [CrossRef] [PubMed]
45. Carlier, J.; Diao, X.; Scheidweiler, K.B.; Huestis, M.A. Distinguishing intake of new synthetic cannabinoids ADB-PINACA and 5F-ADB-PINACA with human hepatocyte metabolites and high-resolution mass spectrometry. *Clin. Chem.* **2017**, *63*, 1008–1021. [CrossRef] [PubMed]
46. Carlier, J.; Diao, X.; Wohlfarth, A.; Scheidweiler, K.B.; Huestis, M.A. In vitro metabolite profiling of ADB-FUBINACA, a new synthetic cannabinoid. *Curr. Neuropharmacol.* **2017**, *15*, 682–691. [CrossRef] [PubMed]
47. Diao, X.; Huestis, M.A. Approaches, challenges, and advances in metabolism of new synthetic cannabinoids and identification of optimal urinary marker metabolites. *Clin. Pharmacol. Ther.* **2017**, *101*, 239–253. [CrossRef] [PubMed]
48. Diao, X.; Huestis, M.A. New synthetic cannabinoids metabolism and strategies to best identify optimal marker metabolites. *Front. Chem.* **2019**, *7*, 109. [CrossRef] [PubMed]
49. Nóbrega, L.; Dinis-Oliveira, R.J. The synthetic cathinone α-pyrrolidinovalerophenone (α-PVP): Pharmacokinetic and pharmacodynamic clinical and forensic aspects. *Drug Metab. Rev.* **2018**, *50*, 125–139. [CrossRef] [PubMed]